Carbogen Inspiration Enhances Hemodynamic Contrast in the Cancerous Breast

Rabah Al abdi[1], Harry L. Graber[1,2], and Randall L. Barbour[1,2]

[1]SUNY Downstate Medical Center,450 Clarkson Ave, Brooklyn NY 11203

[2]NIRx Medical Technologies LLC, 15 Cherry Lane, Glen Head NY 11545, USA

Abstract:

We have explored the vascular response of the breast to inspiration of Carbogen. Results show greater changes in vasoconstriction and hemoglobin oxygen saturation (HbSat) in the tumor-bearing breast compared to the healthy contralateral breast of the same patient.

Introduction:

Key hallmarks of the tumor phenotype are increased stiffness [1], enhanced angiogenesis with sluggish perfusion [2], increased vascular leakiness leading to increased interstitial pressure [3], and increased metabolic demand [2]. Separately, it is known that the vascular autoregulation mechanism achieves a tight coupling between the vascular supply and prevailing metabolic demand. Additionally, it is appreciated that the fidelity of vascular autoregulation may be attenuated in tumor tissue as a consequence of alterations in the peripheral effector complex comprising the vascular endothelium and surrounding vascular smooth muscle [2].

A consequence of the preceding tumor properties is that many tumor types operate on the brink of hypoxemia, suggesting that the otherwise enhanced supply actually is limited, perhaps as a consequence of disturbances in hydrostatic pressures caused by vascular leakiness, and of changes to the interstitial scaffolding [1].

A simple consideration that embraces all of these elements is the expectation that manipulations of the oxygen supply-demand balance could produce responses that differ markedly between the tumor and surrounding healthy tissue. One approach that has recently been considered is the inspiration of carbogen [4]. The response to carbogen is tissue-specific, likely reflecting the differential sensitivity of chemoreceptors and differences in reserve autoregulatory capacity, among other factors. While the typical carbogen response is vasodilation, as a consequence of the effects of elevated CO_2, elevated oxygen levels *per se* typically cause vasoconstriction [4].

In this report we have explored the response of the healthy and tumor-bearing breast to a reduced carbogen mixture, at rest and in response to controlled articulation maneuvers, as a basis for producing additional modulation on the oxygen supply-demand balance.

Methods:

Simultaneous bilateral breast imaging was performed using the optomechanical imaging system recently described by Al abdi *et al*. [5]. The system provides for high-density dynamic optical tomographic imaging and simultaneous measures of the viscoelastic response to precise articulation. Fig. 1a shows a photograph of the two sensing heads used for simultaneous dual-breast measurements, with silicone calibration phantoms in place.

After obtaining informed consent and a brief medical history from the research participants, they were seated and the sensing heads were adjusted to make good contact with both breasts. Following a five-minute baseline scan while breathing room air, a non-rebreathing facemask was applied and subjects breathed a modified carbogen mixture consisting of 98% O_2 and 2% CO_2 for an additional five minutes. A schematic indicating the experimental protocol that extends for 10 minutes is presented in figure 1(b).

Optical data were analyzed offline, using the Normalized Difference Method to reconstruct wavelength-dependent response images [6]. Prior to reconstruction, data were filtered using a low-pass filter with a 0.2-Hz cutoff frequency. The computed wavelength-dependent response was transformed into changes in hemoglobin concentration by solving a 2×2 system of linear equations [7].

Volume-averaged HbSat and total hemoglobin (HbT) time series were calculated by averaging over all finite element mesh nodes (3908 nodes). Statistical tests were performed on the paired differences between image results (Healthy controls: $X_{Left}-X_{Right}$; cancer and benign-pathology subjects: $X_{Affected\ breast} - X_{Unaffected\ breast}$).

A pair of uncorrelated hemodynamic variables (i.e., two orthogonal linear combinations of HbT and HbSat) was generated by projecting the mean-subtracted HbT and HbSat onto the eigenvectors of the HbT-HbSat covariance matrix [8]. Each resulting variable then was normalized to its standard deviation, yielding a distribution with mean zero and unit variance.

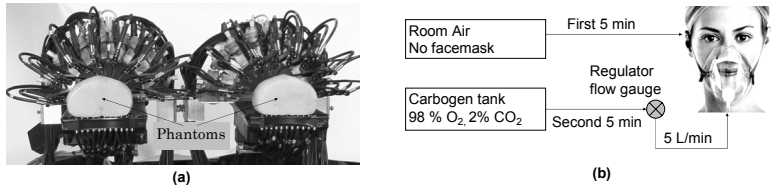

Fig. 1 (a) a photograph of the two sensing heads used for simultaneous dual-breast measurements with phantoms placed in place, (b) schematic indicating the 10-minute experimental protocol.

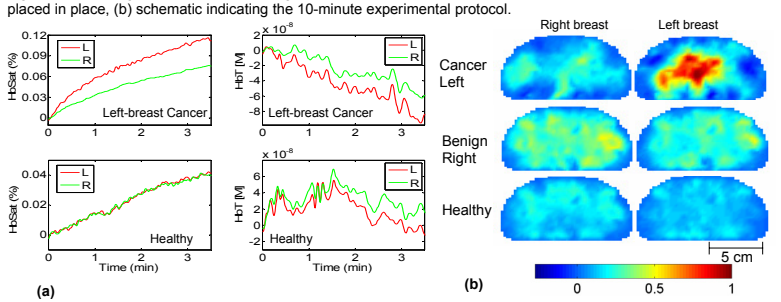

Fig. 2 (a) volume-averaged HbSat and HbT time series. (b) Coronal sections of the HbSat spatial distribution after carbogen inhalation. Images are normalized to the maximum absolute value across subjects. Cancer: 41 y/o, BMI = 27, with 2 cm intra-lobular carcinoma in the left breast; Benign: 48 y/o, BMI = 46, with fibrocystic changes in the right breast. Healthy: 43 y/o, BMI = 35.

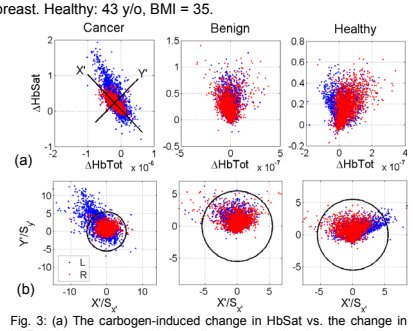

Fig. 3: (a) The carbogen-induced change in HbSat vs. the change in HbT (with respect to the baseline mean values), and (b) linear transform (Mahalanobis distance [8]) of the data in (a) that permits straightforward evaluation of each data point's statistical distance from the mean (HbT, HbSat) values. Circles show critical values for defining outliers.

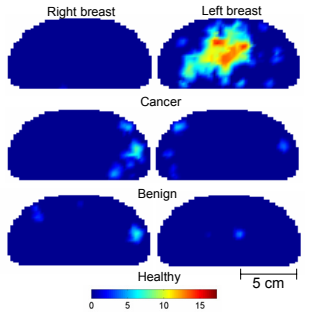

Fig. 4: Coronal sections of statistical distance, thresholded at 5.5 SD. Same subjects as in Fig. 2.

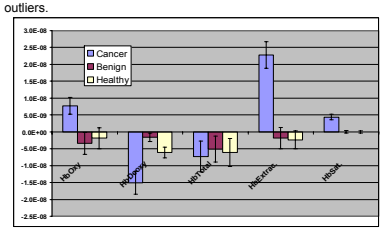

Fig. 5: Mean and standard error of the paired difference between changes in hemoglobin response before and after carbogen breathing. For display purpose: HbSat is scaled by 10^{-7}.

Table 1: patients' clinical information

Category	Age (years)	BMI (kg/m²)
Active cancer (n = 16)	50.8 ± 9.3	33.1 ± 7.8
Benign pathologies (n = 22)	48.2 ± 9.5	33.3 ± 6
Healthy (n = 15)	53.5 ± 11.5	32.6 ± 3.4

Cancer group: IDC (n = 10), invasive mammary carcinoma (n=2), intraductal carcinoma (n = 1), invasive lobular carcinoma (n = 1), ductal carcinoma in situ (n = 1), invasive mucinous carcinoma with extensive DCIS (n = 1). The smallest cancerous tumor was 0.5 cm and the largest was 5 cm.

Table 2: statistical analysis of the paired difference in ΔHbSat.

Group	AUC	Sensitivity (%)	Specificity (%)
Cancer vs. benign	0.85	75	78
Cancer vs. healthy	0.90	88	80
Cancer vs. benign and healthy	0.87	75	70

Results:

Fig. 2 shows volume-averaged HbSat and HbT time series, derived from data collected from cancer and healthy subjects. Cancer subject was 41 y/o, with a BMI of 27 and a 2-cm intra-lobular carcinoma in the left breast, and the healthy subject was 43 y/o with a BMI of 35. It is observed in Fig. 2(a) that HbT levels decrease, indicating a vasoconstrictive response. Both trends in Fig. 2a are physiologically reasonable, given the large increase in the oxygen content of the inspired gas.

Shown in Fig. 2b are axial, sagittal, and coronal views of HbSat changes upon application of carbogen in three subjects: cancer and healthy as Fig. 2a, and a benign breast pathology subject who was 48 y/o with a BMI of 46 and fibrocystic changes in the right breast. The HbSat contrast maps were determined by computing the difference between the mean of HbSat values after the subjects had breathed carbogen for four minutes and the HbSat seen during the baseline period while the subject was breathing room air. Inspection reveals that the region undergoing the largest increase in HbSat coincides closely with the known tumor location, while images of the healthy subject reveal more homogeneous responses in both breasts.

Fig. 3 shows the method we implemented to combine the information from HbTot and HbSat using the Mahalanobis (or statistical) distance. A threshold with 5.5 SD was used to enhance the image contrast.

Fig.4 shows axial, sagittal, and coronal 2D sections of the 3D images with the 5.5 SD threshold applied. Inspection reveals enhanced localization of the breast tumor.

Fig. 5 shows the mean and standard deviation of the paired difference between the volume-averaged HbSat for 16 cancer patients, 22 benign breast-disease subjects, and 15 healthy controls. Inspection reveals significantly different responses for oxyhemoglobin (HbO), deoxyhemoglobin (HbD), hemoglobin oxygen extraction (i.e., HbO – HbD), and HbSat.

Table 2 shows the ROC results (sensitivity, specificity, and accuracy) for the paired HbSat differences among the three groups. Very good accuracy and discriminatory diagnostic power are shown.

Summary:

Results we obtained are consistent with the motivating hypothesis that carbogen and room air would have differential impacts on healthy and tumor tissues' microvasculature. In particular, we have found that tumor tissue shows a larger rise in HbSat in comparison to healthy tissue. One plausible explanation for the enhanced response of cancerous tissue is an aberrant compensatory response in the tumor microvasculature, which in healthy tissue seek to maintain HbSat within a physiologically optimal range.

References:

[1] S. Kumar and V.M. Weaver, "Mechanics, malignancy, and metastasis: the force journey of a tumor cell," *Cancer Metastasis Rev.* **28**, 113-127 (2009).

[2] P. Vaupel, F. Kallinowski, and P. Okunieff, "Blood flow, oxygen and nutrient supply, and metabolic microenvironment of human tumors: a review," *Cancer Res.* **49**, 6449-6465 (1989).

[3] R.E. Hendrick, "Contrast agents in breast magnetic resonance imaging," in *Breast MRI, Fundamentals and Technical Aspects* (Springer, 2008), Chap. **8**, 113-134.

[4] C.M. Carpenter, R. Rakow-Penner, S. Jiang, B.L. Daniel, B.W. Pogue, G.H .Glover, and K.D Paulsen, "Inspired gas-induced vascular change in tumors with magnetic-resonance-guided near-infrared imaging: human breast pilot study," *J. Biomedical Optics* **15**, 036026 (2010).

[5] R. Al abdi, H.L. Graber, Y. Xu, and R.L. Barbour, "Optomechanical imaging system for breast cancer detection," *J. Optical Society of America A*, **28**, 2473-2493 (2011).

[6] Y. Pei, H.L. Graber, and R.L. Barbour, "Influence of systematic errors in reference states on image quality and on stability of derived information for DC optical imaging," *Applied Optics* **40**, 5755-5769 (2001).

[7] J. Choi, M. Wolf, V. Toronov, U. Wolf, C. Polzonetti, D. Hueber, L.P. Safonova, R. Gupta, A. Michalos, W. Mantulin, and E. Gratton, "Noninvasive determination of the optical properties of adult brain: near-infrared spectroscopy approach," *J. Biomedical Optics* **9**, 221–229 (2004).

[8] J. Jomier, V. LeDigarcher, and S. R. Aylward, "Automatic vascular tree formation using the Mahalanobis distance," *Medical Image Computing and Computer-Assisted Intervention LNCS* **3750**, 806-812 (2005).

Acknowledgements:

This research was supported by the National Institutes of Health (NIH) grant R41CA096102, the U.S. Army grant DAMD017-03-C-0018, the Susan G. Komen Foundation, the New York State Department of Health (Empire Clinical Research Investigator Program), and by the New York State Foundation for Science, Technology and Innovation-Technology Transfer Incentive Program (NYSTAR-TIPP) grant C020041.